NANO LETTERS

Subscriber access provided by KANAZAWA UNIV

Letter

Protein#Protein Interactions in Reversibly Assembled Nanopatterns

Tomas Rakickas, Martynas Gavutis, Annett Reichel, Jacob Piehler, Bo Liedberg, and Ramu#nas Valiokas

Nano Lett., **2008**, 8 (10), 3369-3375 • DOI: 10.1021/nl801892m • Publication Date (Web): 13 September 2008

Downloaded from http://pubs.acs.org on December 8, 2008

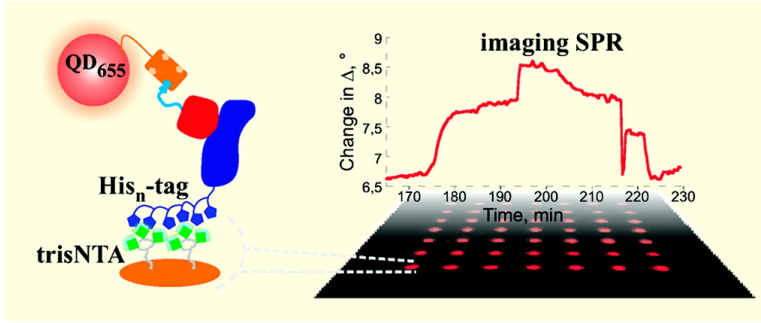

More About This Article

Additional resources and features associated with this article are available within the HTML version:

- Supporting Information
- Access to high resolution figures
- Links to articles and content related to this article
- Copyright permission to reproduce figures and/or text from this article

View the Full Text HTML

ACS Publications
High quality. High impact.

Nano Letters is published by the American Chemical Society. 1155 Sixteenth Street N.W., Washington, DC 20036

NANO LETTERS

2008
Vol. 8, No. 10
3369-3375

Protein−Protein Interactions in Reversibly Assembled Nanopatterns

Tomas Rakickas,[†] Martynas Gavutis,[†] Annett Reichel,[‡] Jacob Piehler,[‡] Bo Liedberg,[§] and Ramūnas Valiokas*,[†]

Department of Functional Nanomaterials, Institute of Physics, Savanorių 231, LT-02300 Vilnius, Lithuania, Institute of Biochemistry and Cluster of Excellence Macromolecular Complexes (CEF), Johann Wolfgang Goethe-University, Max-von-Laue-Strasse 9, 60438 Frankfurt, Germany, and Division of Molecular Physics, Department of Physics, Chemistry, and Biology, Linköping University, 58183 Linköping, Sweden

Received June 30, 2008; Revised Manuscript Received August 20, 2008

ABSTRACT

We describe herein a platform to study protein−protein interactions and to form functional protein complexes in nanoscopic surface domains. For this purpose, we employed multivalent chelator (MCh) templates, which were fabricated in a stepwise procedure combining dip-pen nanolithography (DPN) and molecular recognition-directed assembly. First, we demonstrated that an atomic force microscope (AFM) tip inked with an oligo(ethylene glycol) (OEG) disulfide compound bearing terminal biotin groups can be used to generate biotin patterns on gold achieving line widths below 100 nm, a generic platform for fabrication of functional nanostructures via the highly specific biotin−streptavidin recognition. Subsequently, we converted such biotin/streptavidin patterns into functional MCh patterns for reversible assembly of histidine-tagged (His-tagged) proteins via the attachment of a tris-nitriloacetic acid (trisNTA) biotin derivative. Fluorescence microscopy confirmed reversible immobilization of the receptor subunit ifnar2-His_{10} and its interaction with interferon-α2 labeled with fluorescent quantum dots in a 7 × 7 dot array consisting of trisNTA spots with a diameter of ∼230 nm. Moreover, we carried out characterization of the specificity, stability, and reversibility as well as quantitative real-time analysis of protein−protein interactions at the fabricated nanopatterns by imaging surface plasmon resonance. Our work offers a route for construction and analysis of functional protein-based nanoarchitectures.

Artificial molecular architectures that utilize and/or mimic the building blocks of living cells constitute a fascinating area of nanoscience and nanotechnology. They have a huge potential for applications in bioelectronics, biomedicine, and biotechnology. Functional biological entities like proteins that are responsible for energy conversion in the cell (e.g., photosynthetic complexes, ATP synthases) already have been employed in fabrication of hybrid photosynthetic devices[1,2] and molecular motors.[3,4] However, recent progress in high-resolution electron tomography has revealed that many proteins in the cell are organized into transient nanostructures.[5] A prominent example is the nuclear pore complex, which is formed by a dynamic assembly of several hundred proteins.[6] These complexes perform highly regulated, bidirectional exchange of RNA and proteins between the cytosol and the nucleus, and they are extremely difficult to study because of their dynamic nature and susceptibility to the local membrane environment, that is, the nuclear envelope. Mimicking similar complicated protein architectures and networks in vitro would enable systematic approaches to explore cooperative biological processes. Moreover, fabrication of machineries based on multiple biological components could be envisaged, for example, new molecular cargo devices, precision drug delivery systems, and biosensors. Therefore, nanopatterning and manipulation of proteins on solid surfaces[7−9] is a timely and challenging task. However, the progress in this field until very recently has been limited by the lack of tools to directly interface different functional proteins and to probe the specific protein−protein interactions in artificial nanoarchitectures.

One very promising technique for controlled nanoscale patterning of solid surfaces relies on direct transfer of bifunctional molecules using dip-pen nanolithography (DPN).[10] It is based on diffusion of molecules from the atomic force microscope (AFM) tip to the surface.[11] This process allows arraying of multiple molecular inks over centimeter-sized surface areas, achieving sub-50 nm resolution.[12,13] DPN has proven successful for patterning of

* To whom correspondence should be addressed. E-mail: valiokas@ar.fi.lt. Phone: +370 5 2661640. Fax: +370 5 2602317.

[†] Department of Functional Nanomaterials, Institute of Physics, Savanorių 231, LT-02300 Vilnius, Lithuania.

[‡] Institute of Biochemistry and Cluster of Excellence Macromolecular Complexes (CEF), Johann Wolfgang Goethe-University, Max-von-Laue-Str. 9, 60438 Frankfurt, Germany.

[§] Division of Molecular Physics, Department of Physics, Chemistry and Biology, Linköping University, 58183 Linköping, Sweden.

10.1021/nl801892m CCC: $40.75 © 2008 American Chemical Society
Published on Web 09/13/2008

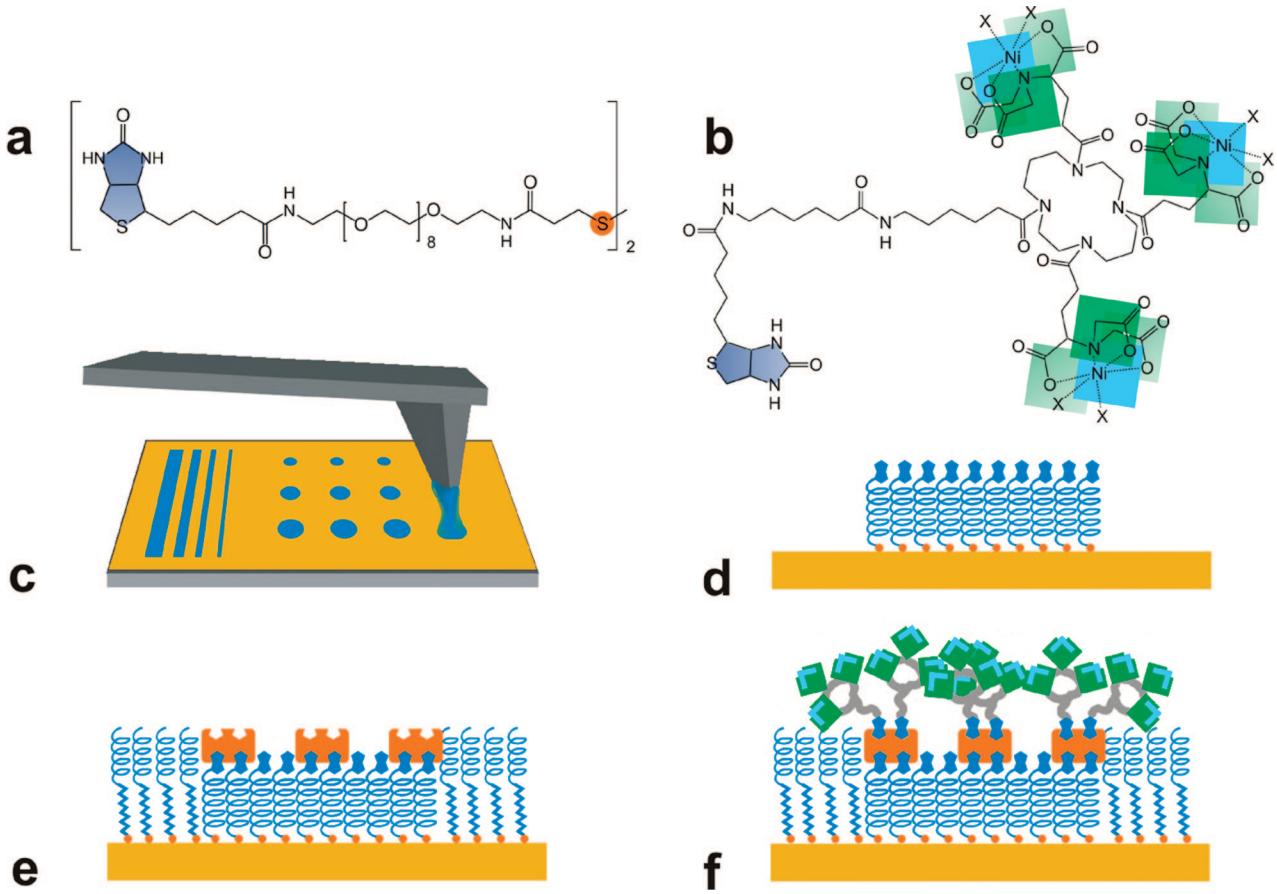

Figure 1. Chemical structures of (a) biotin-disulfide used as an ink in dip-pen nanolithography (DPN) and (b) trisNTA biotin derivative (^{BT}trisNTA) for formation of multivalent chelator (MCh) domains. (c-d) Strategy for fabrication of MCh nanoarrays for the reversible immobilization of His-tagged proteins. (c) DPN fabrication of patterns of lines and dots on gold using biotin-disulfide as ink. (d) Schematic representation of an idealized self-assembled monolayer domain with terminal biotin groups formed from the compound shown in panel a after the DPN printing. (e) Backfilling of the DPN-fabricated pattern with an oligo (ethylene glycol) thiol or disulfide and subsequent specific immobilization of streptavidin to biotin groups. (f) Formation of a multivalent chelator domain via molecular recognition-driven self-assembly of ^{BT}trisNTA on the streptavidin/biotin patterns.

functional proteins, for example, antibodies,[14,15] enzymes,[16] integrins[17] and photosynthetic complexes.[18] However, most of the previous works relies on covalent immobilization or sometimes simple physisorption of proteins. Covalent strategies to build protein nanoarchitectures in particular suffer from several limitations, such as an increased risk of denaturation of proteins and/or unfavorable orientation and presentation of their binding epitopes. Thus, reversible interfacing and multiplexing of different proteins into functional nanodomains via specific tags would be an important step for the fabrication more complex protein nanoarchitectures. Although several well-established strategies exist for immobilization of tagged proteins onto homogeneous biosensor surfaces (for example, histidine (His)-tagged proteins can be reversibly recruited via the nickel ion-chelating nitriloacetic acid (NTA) group), they can hardly be applied at nanoscale because of rapid dissociation. The solution to this fundamental problem has been very recently offered by introducing the tris-nitrilotriacetic acid (trisNTA), a multivalent chelator (MCh), which shows a more than thousand-fold higher affinity for His-tags than the conventional monoNTA group.[19,20]

In this letter, we report on the combination of the two powerful instrumental and molecular tools to fabricate nanopatterns for probing of protein−protein interactions, the first critical step toward formation of functional multiprotein complexes. Namely, in a stepwise procedure (Figure 1), we first take advantage of DPN to generate biotin patterns on gold, using a disulfide oligo(ethylene glycol) ink with terminal biotin groups. Next, we use the biotin/streptavidin platform for molecular recognition-mediated assembly of a biotinylated tris-nitrilotriacetic acid (^{BT}trisNTA) derivative[20] on the DPN-fabricated patterns. We show that the obtained MCh templates are suitable for reversible formation of functionally active His-tagged receptor nanopatterns very much like MCh microarrays previously fabricated by ink-jet printing,[21−23] a practical implication for constructing protein nanoarrays for multiple use. Moreover, we employ imaging surface plasmon resonance (iSPR) to characterize the specificity of protein binding as well as to perform quantitative analysis of protein−protein interactions in the fabricated nanopatterns in real time. On the basis of these measurements, our work provides decisive evidence that the trisNTA groups in molecular nanoarchitectures can be used

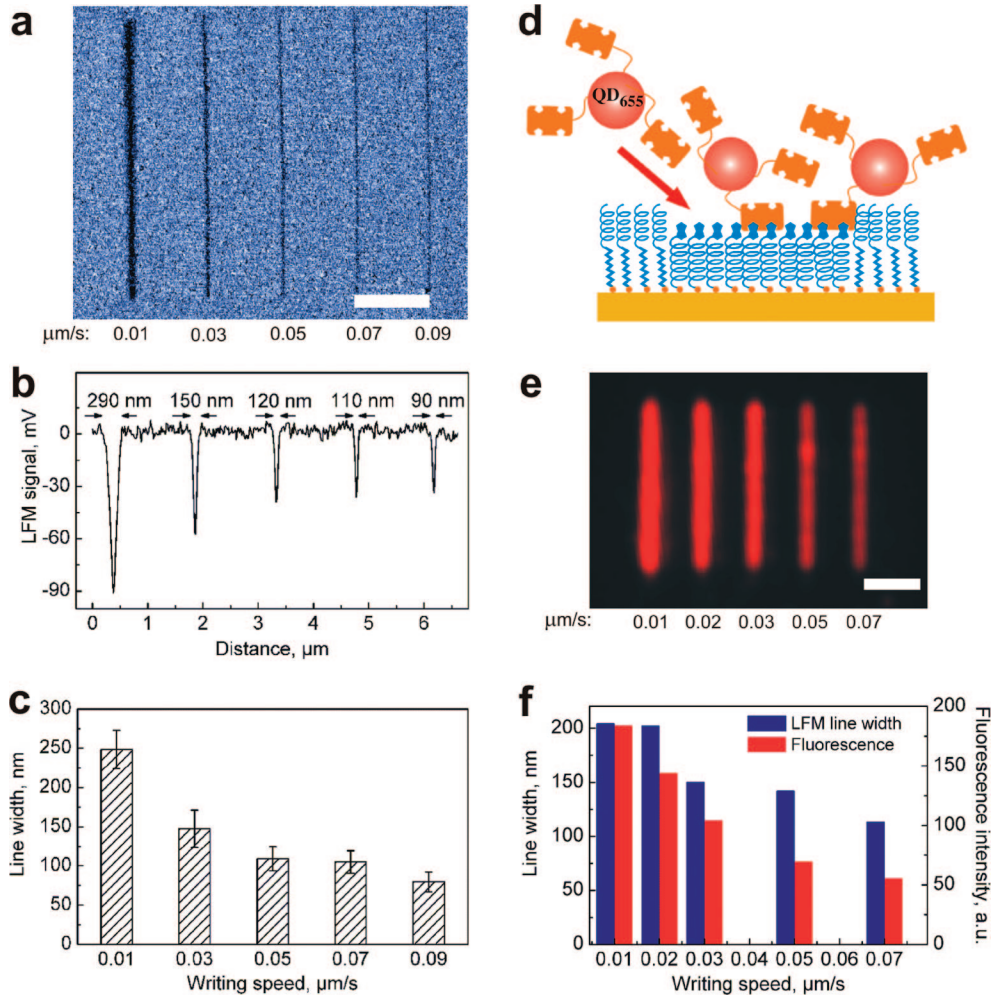

Figure 2. (a) LFM image of lines on gold generated by DPN with biotin-disulfide derivative as ink operating at five different writing speeds. The scale bar is 1.5 μm. (b) Thickness of biotin lines shown in panel a measured as integrated lateral force signal. (c) Averaged line width as function of the writing speed. The line width was obtained from integrated lateral force signals of identical biotin nanopatterns, each fabricated on a different sample. The error bars show standard deviation, $n = 5$. (d) Cartoon illustrating the specific immobilization of quantum dots QD_{655} modified with streptavidin (streptavidin-QD_{655}) on the biotin-terminated patterns on gold surface obtained by DPN and blocking with thiol-oligo(ethylene glycol) compounds (see text for details). (e) Epifluorescence microscopy image of an array of lines similar to those shown in panel a after the immobilization of streptavidin-QD_{655} conjugate as described in panel d. (f) Comparison of the biotin line width measured by LFM directly after DPN writing and the fluorescence intensity of the immobilized streptavidin-QD_{655}, respectively, for the sample shown in panel e.

for stable and oriented positioning of reversible His-tagged receptor−ligand assemblies.

Dip-Pen Nanolithography Using Biotin-disulfide As Ink. A variety of inks has been shown to be compatible with the DPN fabrication.[12] However, diffusion of complex, charged and strongly interacting molecular entities like the MChs and their assembly on surfaces is a complicated and not yet fully understood process. For example, we have found that DPN employed directly on gold using a set of multivalent NTA-terminated thiol inks[23] creates nanostructures, which do not display the specificity to His-tagged proteins (not shown). Therefore, to obtain functional MCh domains we have chosen to employ a two step process combining DPN and the well-known biotin-streptavidin platform. Previously, biotin nanopatterns on gold and silicon oxide surfaces have been fabricated via in situ reactions of biotin derivatives with DPN patterned thiol[24] and silane[25] inks, respectively, which contained reactive terminal groups. Also, DPN patterning of a bifunctional biotin-maleimide compound on thiol-terminated silane surfaces recently has been reported.[26] However, writing with the biotin-disulfide ink (Figure 1) turned out to be an interesting alternative, as it allowed a direct fabrication of biotin nanoarrays on gold. Figure 2a shows a lateral force microcopy (LFM) image obtained at a scanning speed of 40 μm/s directly after having written lines at several different writing speeds ranging from 0.01 to 0.09 μm/s. Integrated lateral force signal analysis of the LFM image (Figure 2b) is used to measure the width of the fabricated biotin lines, which gradually decrease from 290 to 90 nm, respectively. Also, the decreasing amplitude of the negative peaks in the LFM signal is a qualitative indication of the decreasing amount of the ink transferred to the surface with increasing writing speed. The most reproducible DPN features were obtained at a relative humidity of around 50%, and it was necessary to stabilize the diffusion of the biotin-disulfide ink via writing on dummy

areas before fabrication of the desired features. Having removed excess of biotin-dislufide ink, we could carry out the printing process for up to five hours with reproducible line width (Figure 2c).

A direct quantification of the biotin-disulfide in the generated DPN features via measuring their height with AFM in contact mode was not possible because of the cross-talk between the vertical motion of the scanning tip and its lateral interactions with the surface[25] and also because the inspection of the fabricated sample was carried out at a high scanning speed to avoid the contamination with the ink. Therefore, we could perform only an indirect, relative comparison of the biotin amount in the lines obtained at different writing speeds by observing the attachment of streptavidin labeled with quantum dots using fluorescence microscopy (Figure 2d). In this series of experiments, the samples were patterned with biotin-disulfide ink as described above, and the remaining nonpatterned Au surface area was blocked with an oligo(ethylene glycol) (OEG) thiol derivative, $HS(CH_2)_{11}O-(CH_2CH_2O)_7$-H, to suppress the nonspecific adsorption of proteins. Then the samples were incubated with streptavidin-functionalized quantum dots (QD_{655}). Figure 2e shows a typical fluorescence image of a pattern of lines obtained under similar conditions as for the samples discussed above. It confirms that the amount of the immobilized streptavidin-QD_{655} conjugate decreases with increasing writing speed from 0.01 to 0.07 μm/s. A comparison of the fluorescence intensity and the line widths measured for this particular sample by LFM directly after DPN (not shown) reveals that although both parameters monotonically decrease with increasing writing speed, there is no strict correlation between the line width and the amount of the biotin groups capable to bind the streptavidin-functionalized QD_{655} (Figure 2e). Moreover, the line width dependence on the inverse writing speed (not shown) is nonlinear, a finding that is in agreement with previous reports using mercaptohexadecanoic acid and octadecane thiol as inks.[27,28] Our finding as well as those in the cited works suggest a complex diffusion of the biotin-disulfide ink from the AFM tip to the substrate, which needs further investigations, for example, to explore the influence of humidity, temperature, modification of the AFM tip[27−31] or ink composition.[26] It is noteworthy that a tip bias of +7 V enabled us to increase the writing speed more than 10 times. This was advantageous when relatively large patterned surface areas were needed for the iSPR measurements (see below).

Fabrication of His-tagged Protein Nanopatterns. In the next series of experiments, we employed DPN to print biotin-terminated dot arrays for the assembly of MChs. Keeping in mind the limited detection sensitivity of the optical method used in this study for functional characterization of the His-tagged proteins, we fabricated the arrays with features sizes larger than 200 nm. In the printing process, we brought the AFM tip inked with the biotin-disulfide into a contact with the gold surface for 60 s, a typical contact time for achieving a sufficiently high density of the biotin groups in the dots for the detection of labeled fluorescent proteins. After having blocked the nonprinted parts with the OEG, we incubated the sample in a solution of streptavidin and subsequently in a solution of the ^{BT}trisNTA conjugate, Figure 1. Note that such a noncovalent attachment of the prepared MChs has the advantages over recently reported covalent immobilization of protected trisNTA as the latter strategy requires deprotection of the carboxyl groups using aggressive agents such as trifluoracetic acid.[32] The use of similar reactive reagents is critical keeping in mind the risk of damaging the nanofabricated assemblies and/or potentially increased nonspecific protein binding. Thus, the stepwise procedure allowed us to generate an array of MCh (trisNTA) domains, loaded with Ni(II) ions, which could be employed for subsequent attachment of recombinant proteins, for example, the ectodomain of the type I interferon receptor subunit ifnar2 fused to a C-terminal decahistidine tag (ifnar2-His_{10}). To inspect a fabricated trisNTA 7 × 7 dot array and to verify the functional activity of the immobilized ifnar2-His_{10}, we probed its interaction with interferon IFNα2 labeled with QD_{655}.[9] The schematic representation and the result of the assay, epifluorescence microscopy images of functionally active ifnar2-His_{10} immobilized on the trisNTA domains, are shown in Figure 3. The assay reveals that binding of the IFNα2-QD_{655} conjugates in the array spots is specific, as virtually no fluorescence is seen in the protein repellent regions consisting of the OEGs. Moreover, the fluorescent pattern completely disappears upon exposing the sample to 1 M solution of imidazole, which competes with the His-tagged protein in the trisNTA domains. Subsequently, the sample was washed extensively with buffer, reloaded with Ni(II) and subsequently with ifnar2-His_{10}, followed by binding of the IFNα2-QD_{655} conjugate. Figure 3d reveals a significant recovery of the fluorescence intensity, which is measured to be about 70% with respect to the first loading. Note that such a functional assay using the IFNα2-QD_{655} conjugate as a ligand cannot be used for quantitative estimation of the reversibility of the created His-tagged protein nanopatterns. For instance, the observed loss of the fluorescence intensity in the subsequent loading, which unfortunately must be undertaken ex-situ, can be due to a possible irreversible contamination of the trisNTA groups with impurities and degradation products from the protein-QD_{655} conjugate solution.

After the functional experiment with proteins, we removed them by treating 7 × 7 trisNTA dot nanoarray with 100 mM HCl. The sample was then investigated with AFM in air in order to estimate the typical sizes of the biotin domains generated by DPN (Figure 3e).[33] The analysis of the obtained phase images reveals that the analyzed array consisted of dots with a size of 234 ± 17 nm.

Characterization of Assembly and Quantitative Analysis of Protein−Protein Interactions. We employed iSPR, which is a label-free detection method, to characterize the reversible assembly of the His-tagged proteins to the generated trisNTA templates as well as to analyze quantitatively protein−protein interactions at the nanopatterns. This method allowed us to follow, in real time, the adsorption of molecular entities as well as the interaction between the immobilized

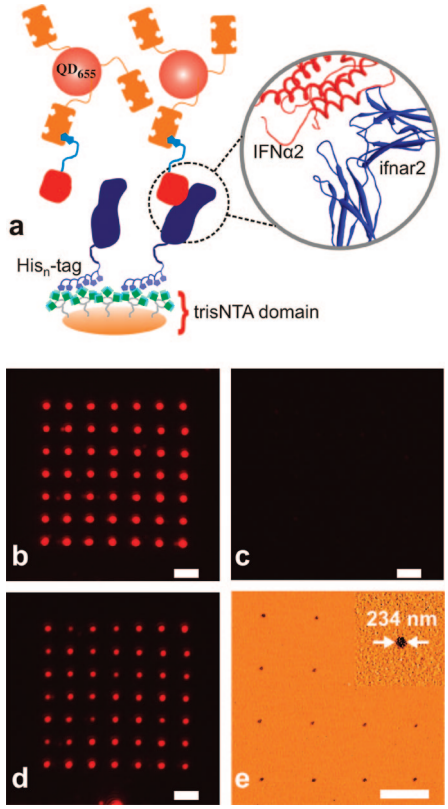

Figure 3. (a) Schematic representation of the fluorescence assay for detection of the specific interaction between ifnar2-His_{10} and IFNα2 in the trisNTA nanoarray (not to scale). In this assay, IFNα2 is labeled with fluorescent quantum dots (QD_{655}). The close-up image is a fragment of a molecular model obtained by NMR analysis of the IFNα2-ifnar2 complex.[34] (b−d) Epifluorescence micrographs showing the functional activity of ifnar2-His_{10} receptors assembled on the trisNTA nanoarray using the assay described in panel a. (b) TrisNTA array after loading ifnar2-His_{10} and subsequently incubating it with IFNα2-QD_{655} conjugate. (c) The same array after rinsing in 1 M imidazole. (d) The trisNTA array was reloaded with ifnar2-His_{10} and exposed to IFNα2-QD_{655}. (e) Phase image obtained by tapping mode atomic force microscopy showing a part of the same array after the removal of proteins by 100 mM HCl. The inset shows a close-up of one of the array spots. The scale bar in panels b−e is 3 μm.

ifnar2-His_{10} and IFNα2 in selected regions of interest (ROIs). The maximal lateral resolution of iSPR is defined by the propagation length of the surface plasmon,[35] which for the present setup was less than 1 μm. However, we found that in practice ROIs of 10 μm were necessary to record the association and dissociation phases with acceptable signal-to-noise ratio. Namely, the actual resolution of the iSPR was affected by the instrumental factors such as the optical resolution of objective used, sensitivity to mechanical vibrations, nonuniform sample illumination caused by laser interference fringes, sample position drift because of thermal effects and/or changing properties of optical index-matching oil (the apparent drift was about 2 μm in 4 h).

The sample preparation and iSPR experiments are described in more detail in Supporting Information. Briefly, prior to DPN, the gold-coated substrates for iSPR were microcontact printed (μCP) with eicosanethiol (HSC_{20}) to create a hydrophobic grid defining working areas (squares) up to 50 × 50 μm^2 for DPN. The grid also served as a reference for quantification of protein adsorption (see discussion below). Further on, 406 ± 23 nm wide biotin lines with 171 ± 23 nm spacing (mean and sdv) were printed on gold by DPN in a working area of 17 × 17 μm^2 within the grid and the generated pattern was backfilled with an OEG disulfide, $(-S(CH_2)_2(OCH_2CH_2)_6OCH_3)_2$. The sample was incubated with bovine serum albumin (BSA) to block the hydrophobic grid, washed with MilliQ water, and then it was mounted into a Nanofilm EP^3 instrument for iSPR operating in ellipsometric mode. The MCh domains were assembled in situ on the DPN-fabricated biotin line patterns by injecting into the flow cell a mixture of 300 nM streptavidin and 750 nM ^{BT}trisNTA, followed by an additional injection of 1 μM ^{BT}trisNTA. The ^{BT}trisNTA conjugate used in this procedure was preloaded with Ni(II) ions. This procedure was used to obtain a high and reproducible loading of active trisNTA.

To characterize the specificity and reversibility of His-tagged protein binding to the MCh pattern, we first used maltose binding protein fused to a C-terminal decahistidine tag[36] (MBP-His_{10}). Figure 4a shows the kinetics of MBP-His_{10} binding within two different ROIs: the red curve is the kinetics recorded within the DPN-fabricated pattern of lines and the black curve is the control signal from a nonpatterned OEG region. Selective binding of MBP-His_{10} to the MCh pattern was observed with a characteristic shape of the binding curve as previously measured on nonpatterned surfaces.[20] Stable immobilization of the protein to the MCh pattern was observed during several minutes of buffer wash, which is in agreement with the more than thousand-fold higher affinity of trisNTA toward His-tags as compared to monoNTA. Upon injection of 250 mM imidazole, the protein was selectively removed from the surface, and approximately the same amount of MBP-His_{10} was loaded in the next immobilization cycle. These results demonstrate the unique properties of trisNTA templates for repetitive protein immobilization into nanopatterns, which are crucial for the assembly of protein entities into functional complex nanoarchitectures.[23,36,37] The amount of MBP-His_{10} specifically bound in the second cycle was estimated to be approximately 90% as compared to the initial amount. However, after the two MBP-His_{10} immobilization cycles the chip was kept in the flow system for 24 h, and repeated binding experiments were carried out on the next day by immobilizing a different model system, ifnar2-His_{10} (Supporting Information). Reproducible ifnar2-His_{10} amounts ∼0.4 ng mm^{-2} were obtained during the two additional immobilization/regeneration cycles, confirming efficient reversibility of protein assembly formation in MCh nanopatterns. This is in agreement with the previous study by Reichel et al., which also demonstrated the full reversibility of the ^{BT}trisNTA conjugate binding to His-tagged proteins.[20]

To probe the functionality of the immobilized protein, we employed iSPR to characterize the interactions between ifnar2-His_{10} receptor and its ligand IFNα2 in the fabricated trisNTA line patterns. Figure 4b shows a real time monitoring of the ifnar2-His_{10} immobilization as well as its interaction with IFNα2 in an array of lines analogous to that discussed

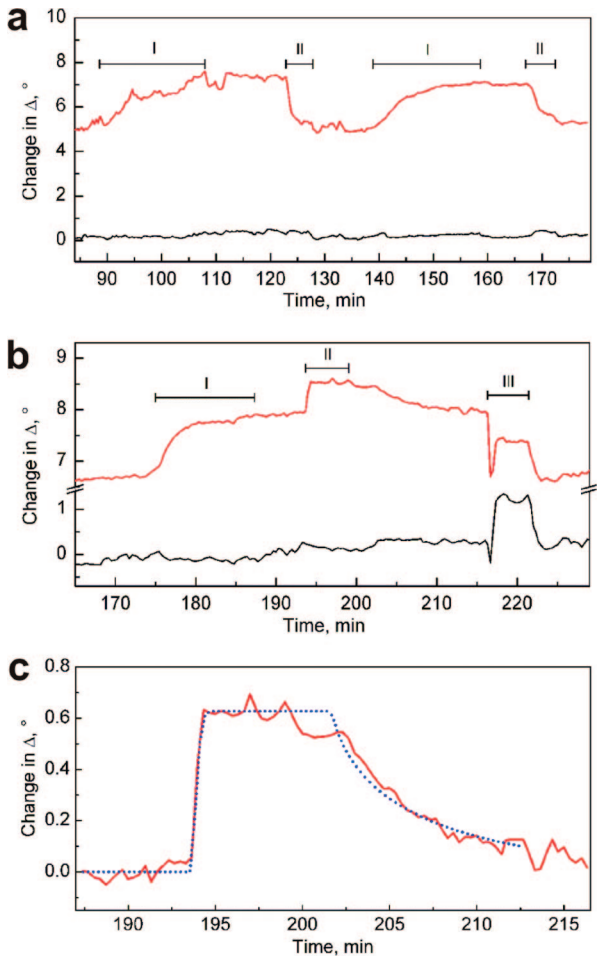

Figure 4. Kinetics of His-tagged proteins binding to trisNTA multivalent chelator groups assembled on biotin patterns fabricated with dip-pen nanolithography probed by iSPR. The kinetics were corrected to have the same baseline slope and subtracted with the reference signal. (a) Reversible immobilization of MBP-His_{10}. The red curve is the Δ signal from a ROI of 14 × 14 μm^2 on a pattern of 406 ± 23 nm lines with 171 ± 23 nm spacing. The black curve is control measurement on an area coated with an oligo(ethylene glycol)-terminated (OEG) self-assembled monolayer (SAM). The injections were I, 500 nM MBP and II, 250 mM imidazole. The observed higher noise in the first immobilization cycle is due to mechanical instabilities of the employed fluidics system. (b) iSPR kinetics (second immobilization cycle) showing a specific attachment and functional activity of ifnar2-His_{10}. The red curve is the Δ signal from a ROI of 16 × 16 μm^2 on a pattern of 364 ± 14 nm lines with 62 ± 11 nm spacing. The black curve is a control measurement on an area coated with an OEG SAM. The injections are the following: I, 500 nM ifnar2-His_{10}; II, 1 μm IFNα2; III, 1 M imidazole. (c) Comparison between the association/dissociation kinetics of IFNα2 (solid red curve, the same kinetics as in panel b and the fit obtained from a receptor−ligand interaction model, which includes the mass transport limitation (dashed blue curve).

previously. Characteristic immobilization kinetics was also observed for ifnar2-His_{10}, yielding a stable binding signal with change in Δ close to 8°. Subsequent addition of 1 μM of IFNα2 resulted in a sharp increase in Δ due to fast association to the binding sites of ifnar2-His_{10} in the trisNTA domains (II), which is consistent with the high association rate constant of the IFNα2-ifnar2 complex.[38,39] Rapid saturation of the binding sites confirmed specificity of the interaction. After the dissociation of the ligand, the sample was successfully regenerated by injection of 1 M imidazole (III). Inspection of the binding curve confirmed pronounced mass transport limitation due to the high association rate constant of the interaction, the relatively high infar2-His_{10} surface concentration required for unambiguous detection and the nonoptimized fluidics system of the iSPR instrument used in these experiments. Nevertheless, the kinetics of the ifnar2-His_{10}/IFNα2 complex formation and dissociation in DPN-fabricated MCh patterns is very similar to that obtained previously for micropatterned samples.[22] The ligand binding curve was fitted by a receptor−ligand interaction model, which included the mass transport limitation using simultaneous fitting of the association and the dissociation kinetics (Figure 4c). This analysis yielded an association rate constant k_a of ∼2 × 10^5 $M^{-1}s^{-1}$ and a dissociation rate constant k_d of ∼1 × 10^{-2} s^{-1}. While the k_d is in perfect agreement with the k_d of this interaction obtained under more optimized conditions (1 × 10^{-2} s^{-1}), a larger deviation is obtained for the k_a (∼1 × 10^6 $M^{-1}s^{-1}$).[38,39] This deviation can be explained by the fact that due to mass transport limitation the association phase of the binding curve contains very little information about the association rate constant (only a few points in the curvature before reaching saturation). Note, that modeling of the ifnar2-His_{10}/ IFNα2 interaction kinetics previously measured in MCh-terminated SAM micropatterns with the same iSPR system[22] yielded a very similar k_a of ∼4 × 10^5 $M^{-1}s^{-1}$ and an identical k_d of ∼1 × 10^{-2} s^{-1} (Supporting Information).

We also took advantage of iSPR to quantitatively estimate the effective protein surface concentrations in the fabricated MCh patterns. We used in iSPR as a reference the height difference between the hydrophobic HSC_{20} grid coated with BSA and the OEG-terminated region of the prestructured DPN samples, which by imaging ellipsometry was determined to equal ∼2 nm (Supporting Information). The corresponding change in the Δ signal measured by iSPR was ∼9°. Thus, assuming the same refractive index for all proteins and a linear relationship between the Δ signal and the thickness of the adsorbed organic layer in this thickness range, the obtained equivalent surface density of streptavidin specifically bound to the biotin lines is approximately 1.6 ng mm^{-2}. Note that this value is corrected for the filling factor of the patterns of lines fabricated by DPN. This surface density is close to the amount of streptavidin obtained on biotin-terminated self-assembled monolayers prepared in solution.[40] Further on, the amount of MBP-His_{10} immobilized in the assembled MCh patterns, estimated from the first immobilization shown in Figure 4a is about 0.8 ng mm^{-2}. Likewise, the functional test shown in Figure 4b reveals the amounts of immobilized ifnar2-His_{10} (∼0.4 ng mm^{-2}) and its ligand IFNα2 (∼0.2 ng mm^{-2}). On the basis of these numbers and the molecular masses of the two interacting proteins, it can be estimated that at least 65% of the immobilized ifnar2-His_{10} is active. This number is in excellent agreement with measurements made on other optimized surfaces.[36,37]

To conclude, we have developed a versatile strategy for construction of functional assemblies of His-tagged proteins, which is based on DPN fabrication, molecular recognition-mediated self-assembly, and molecular multivalency. We have fabricated and characterized MCh nanoarrays in a protein-repellent OEG matrix, and we successfully used these arrays to probe protein−protein interactions. Specific interaction of nanopatterned ifnar2-His_{10} with its ligand IFNα2 was visualized by fluorescence microscopy using functionalized quantum dots as labels. Quantitative functional analysis of His-tagged receptors immobilized in the DPN features by iSPR confirmed that at least two-thirds of the immobilized protein molecules remained functional and displayed ligand binding kinetics, which is typical for this biological model system. This is not trivial for a protein like ifnar2, which is very sensitive toward immobilization and completely denatures upon physisorption onto solid supports.[39] Retaining the function of proteins in artificial nanostructures is a particular challenge for the assembly of functional protein complexes. Thus, our approach offers a versatile route for fabrication of "custom-made" functional assemblies of recombinant proteins by employing natural protein systems or mimicking the functional properties of protein complexes existing in living cells. Next to His-tag specific immobilization, covalently biotinylated proteins possibly could be captured also into these patterns. In the longer perspective, the approach can provide a superior platform for the construction of advanced protein-based machineries.

Acknowledgment. This work was supported by the Lithuanian State Science and Studies Foundation, the Swedish Research Council (VR), the Swedish Foundation for Strategic Research (SSF) and the Swedish Institute through the Visby program. This work was also supported by the German Research Council (DFG, Pi-405/2, Pi-405/4, and EXC 115) and by the German Ministry of Education and Research (BMBF, 0312034A). T.R. acknowledges Graduate School Forum Scientium and a Marie Curie Early Stage Research Training Fellowship of the European Communitys FP6 under contract number MEST-CT-2004-504272. The authors are grateful to Dr. Sofia Svedhem and Dr. Stefan Svensson for synthesizing the OEG thiol compound.

Supporting Information Available: A description of materials and methods, AFM, and SPR images of samples with patterns of lines for protein adsorption kinetics measurements, unmodified imaging SPR kinetics of protein immobilization and interactions in nanopatterns, experimental, and fitted kinetic curves of ifnar2-His_{10}/ IFNα2 interactions in micropatterns. This material is available free of charge via the Internet at http://pubs.acs.org.

References

(1) Das, R.; Kiley, P. J.; Segal, M.; Norville, J.; Yu, A. A.; Wang, L. Y.; Trammell, S. A.; Reddick, L. E.; Kumar, R.; Stellacci, F.; Lebedev, N.; Schnur, J.; Bruce, B. D.; Zhang, S. G.; Baldo, M. *Nano Lett.* **2004**, *4*, 1079–1083.
(2) Frolov, L.; Rosenwaks, Y.; Carmeli, C.; Carmeli, I. *Adv. Mater.* **2005**, *17*, 2434–2437.
(3) Soong, R. K.; Bachand, G. D.; Neves, H. P.; Olkhovets, A. G.; Craighead, H. G.; Montemagno, C. D. *Science* **2000**, *290*, 1555–1558.
(4) van den Heuvel, M. G. L.; Dekker, C. *Science* **2007**, *317*, 333–336.
(5) Robinson, C. V.; Sali, A.; Baumeister, W. *Nature* **2007**, *450*, 973–982.
(6) Beck, M.; Lucic, V.; Forster, F.; Baumeister, W.; Medalia, O. *Nature* **2007**, *449*, 611–615.
(7) Wadu-Mesthrige, K.; Xu, S.; Amro, N. A.; Liu, G. Y. *Langmuir* **1999**, *15*, 8580–8583.
(8) Coyer, S. R.; Garcia, A. J.; Delamarche, E. *Angew. Chem., Int. Ed.* **2007**, *46*, 6837–6840.
(9) Tinazli, A.; Piehler, J.; Beuttler, M.; Guckenberger, R.; Tampe, R. *Nat. Nanotechnol.* **2007**, *2*, 220–225.
(10) Piner, R. D.; Zhu, J.; Xu, F.; Hong, S. H.; Mirkin, C. A. *Science* **1999**, *283*, 661–663.
(11) Jaschke, M.; Butt, H. J. *Langmuir* **1995**, *11*, 1061–1064.
(12) Ginger, D. S.; Zhang, H.; Mirkin, C. A. *Angew. Chem., Int. Ed.* **2004**, *43*, 30–45.
(13) Salaita, K.; Wang, Y. H.; Mirkin, C. A. *Nat. Nanotechnol.* **2007**, *2*, 145–155.
(14) Lee, K. B.; Park, S. J.; Mirkin, C. A.; Smith, J. C.; Mrksich, M. *Science* **2002**, *295*, 1702–1705.
(15) Lee, S. W.; Oh, B. K.; Sanedrin, R. G.; Salaita, K.; Fujigaya, T.; Mirkin, C. A. *Adv. Mater.* **2006**, *18*, 1133–1136.
(16) Hyun, J.; Kim, J.; Craig, S. L.; Chilkoti, A. *J. Am. Chem. Soc.* **2004**, *126*, 4770–4771.
(17) Lee, M.; Kang, D. K.; Yang, H. K.; Park, K. H.; Choe, S. Y.; Kang, C.; Chang, S. I.; Han, M. H.; Kang, I. C. *Proteomics* **2006**, *6*, 1094–1103.
(18) Valiokas, R.; Vaitekonis, A.; Klenkar, G.; Trinkunas, G.; Liedberg, B. *Langmuir* **2006**, *22*, 3456–3460.
(19) Lata, S.; Reichel, A.; Brock, R.; Tampe, R.; Piehler, J. *J. Am. Chem. Soc.* **2005**, *127*, 10205–10215.
(20) Reichel, A.; Schaible, D.; Al Furoukh, N.; Cohen, M.; Schreiber, G.; Piehler, J. *Anal. Chem.* **2007**, *79*, 8590–8600.
(21) Klenkar, G.; Valiokas, R.; Lundstrom, I.; Tinazli, A.; Tampe, R.; Piehler, J.; Liedberg, B. *Anal. Chem.* **2006**, *78*, 3643–3650.
(22) Valiokas, R.; Klenkar, G.; Tinazli, A.; Tampe, R.; Liedberg, B.; Piehler, J. *ChemBioChem* **2006**, *7*, 1325–1329.
(23) Valiokas, R.; Klenkar, G.; Tinazli, A.; Reichel, A.; Tampe, R.; Piehler, J.; Liedberg, B. *Langmuir* **2008**, *24*, 4959–4967.
(24) Hyun, J.; Ahn, S. J.; Lee, W. K.; Chilkoti, A.; Zauscher, S. *Nano Lett.* **2002**, *2*, 1203–1207.
(25) Jung, H.; Kulkarni, R.; Collier, C. P. *J. Am. Chem. Soc.* **2003**, *125*, 12096–12097.
(26) Jung, H.; Dalal, C. K.; Kuntz, S.; Shah, R.; Collier, C. P. *Nano Lett.* **2004**, *4*, 2171–2177.
(27) Schwartz, P. V. *Langmuir* **2002**, *18*, 4041–4046.
(28) Weeks, B. L.; Noy, A.; Miller, A. E.; De Yoreo, J. J. *Phys. Rev. Lett.* **2002**, *88*, 255505.
(29) Sheehan, P. E.; Whitman, L. J. *Phys. Rev. Lett.* **2002**, *88*, 156104.
(30) Rozhok, S.; Piner, R.; Mirkin, C. A. *J. Phys. Chem. B* **2003**, *107*, 751–757.
(31) Peterson, E. J.; Weeks, B. L.; De Yoreo, J. J.; Schwartz, P. V. *J. Phys. Chem. B* **2004**, *108*, 15206–15210.
(32) Turchanin, A.; Tinazli, A.; El-Desawy, M.; Grossann, H.; Schnietz, M.; Solak, H. H.; Tampe, R.; Golzhauser, A. *Adv. Mater.* **2008**, *20*, 471–477.
(33) We did not perform direct AFM analysis of nanoarrays prepared for His-tagged protein binding tests because of increased nonspecific binding of fluorescence-labeled protein to samples, which have been exposed to air.
(34) Quadt-Akabayov, S. R.; Chill, J. H.; Levy, R.; Kessler, N.; Anglister, J. *Protein Sci.* **2006**, *15*, 2656–2668.
(35) Steiner, G. *Anal. Bioanal. Chem.* **2004**, *379*, 328–331.
(36) Lata, S.; Piehler, J. *Anal. Chem.* **2005**, *77*, 1096–1105.
(37) Tinazli, A.; Tang, J. L.; Valiokas, R.; Picuric, S.; Lata, S.; Piehler, J.; Liedberg, B.; Tampe, R. *Chem.−Eur. J.* **2005**, *11*, 5249–5259.
(38) Piehler, J.; Schreiber, G. *J. Mol. Biol.* **1999**, *289*, 57–67.
(39) Piehler, J.; Schreiber, G. *Anal. Biochem.* **2001**, *289*, 173–186.
(40) Nelson, K. E.; Gamble, L.; Jung, L. S.; Boeckl, M. S.; Naeemi, E.; Golledge, S. L.; Sasaki, T.; Castner, D. G.; Campbell, C. T.; Stayton, P. S. *Langmuir* **2001**, *17*, 2807–2816.

NL801892M